JZUS

Dynamic modeling of micro- and nano-sized particles impinging on the substrate during suspension plasma spraying[*]

Kai ZHANG, Hong-bing XIONG[†‡], Xue-ming SHAO[†‡]

(*State Key Laboratory of Fluid Power and Mechatronic Systems, College of Mechanical Engineering,*
Zhejiang University, Hangzhou 310027, China)

[†]E-mail: hbxiong@zju.edu.cn; mecsxm@zju.edu.cn

Abstract: Suspension plasma spraying (SPS) can be utilized to manufacture finely structured coatings. In this process, liquid suspended with micro- or nano-sized solid particles is injected into a plasma jet. It involves droplet injection, solvent evaporation, and discharge, acceleration, heating, and melting of the solid particles. The high-speed and high-temperature particles finally impact on the substrate wall, to form a thin layer coating. In this study, a comprehensive numerical model was developed to simulate the dynamic behaviors of the suspension droplets and the solid particles, as well as the interactions between them and the plasma gas. The plasma gas was treated as compressible, multi-component, turbulent jet flow, using Navier-Stokes equations solved by the Eulerian method. The droplets and solid particles were treated as discrete Lagrangian entities, being tracked through the spray process. The drag force, Saffman lift force, and Brownian force were taken into account for the aerodynamic drag force, aerodynamic lift force, and random fluctuation force imposed on the particles. Spatial distributions of the micro- and nano-sized particles are given in this paper and their motion histories were observed. The key parameters of spray distribution, including particle size and axial spray distance, were also analyzed. The critical size of particle that follows well with the plasma jet was deduced for the specified operating conditions. Results show that in the downstream, the substrate influences the flow field structure and the particle characteristics. The appropriate spray distances were obtained for different micro- and nano-sized particles.

Key words: Suspension plasma spray (SPS), Stokes number, Brownian force, Multiphase flow, Solid-fluid interaction
http://dx.doi.org/10.1631/jzus.A1500203   **CLC number:** O359; TK124

1 Introduction

Suspension plasma spray (SPS) is a novel spray technology (Fauchais, 2004). In the SPS process, the nano-sized particles in the feedstock usually have diameters between 100 nm and 1 μm. These particles are dispersed in suspension and then injected into a plasma flow to form droplets with diameters smaller than 100 μm by atomization devices (Fauchais *et al.*, 2008a). The SPS process involves a series of complex phenomena, such as feedstock injection, suspension breakup (Meillot *et al.*, 2013a; 2013b) and evaporation, and the discharge of particles or their agglomerates into the plasma jet. The solid particles will experience further heating, melting, and evaporation before impacting the substrate. Since the behaviors and states of the particles will affect their coating qualities, it is necessary to understand their dynamic behaviors.

Due to the complex behaviors of the micro- and nano-sized particles, the modeling of SPS becomes difficult. The dynamic behaviors of the particles are dominated by the forces exerted on them. These

forces have been studied using various models (Faeth, 1987; Pfender, 1989; Huang *et al.*, 1995; Jen *et al.*, 2005; Pateyron *et al.*, 2013), mainly using the drag force. Among these models, Jen *et al.* (2005) considered the Brownian force and the Saffman lift force but only in a special flow domain, which is not universal and which introduces errors when used for the spray distribution with sub-micro-sized or nano-sized particles. Thus, it is necessary to use a comprehensive mathematical model to describe the forces affecting the nano-sized particles as well as the micro-sized particles in the plasma field. In this study, we establish a mathematical model to describe the movement of the particles, considering simultaneously the drag force, the Brownian force, and the Saffman lift force for micro- and nano-sized particles during their whole flight in the plasma jet. With the Brownian force, the size effects on the dispersion of the particles are considered, and with the Saffman lift force, the effect of flow shear stress is considered.

In a plasma spray, particle size is a key factor. It will affect the trajectory and thermal state of the particles, especially when considering their interaction with the substrate wall (Jen *et al.*, 2005; Xiong *et al.*, 2005). In presence of the substrate, the flow field and stream traces turn and run parallel to the substrate surface, and thus sufficiently small particles will move with the gas flow and not reach the substrate, while large particles having sufficient inertia will penetrate the boundary layer and reach the substrate surface. The Stokes number is often used to identify the trajectory of particles of different sizes. Crowe *et al.* (1985) firstly studied particle dispersion in free shear flows and concluded that particle dispersion might be strongly dependent on the Stokes number, which is defined as the ratio of particle aerodynamic response time to the time of large scale vortex structures. Since then, the Stokes number has often been used by subsequent researchers to analyze the size effect on the particle movement in the plasma spray process (Crowe *et al.*, 1988; Ye *et al.*, 2000; Jordan *et al.*, 2004; Delbos *et al.*, 2006; Fauchais *et al.*, 2008a; 2008b; Bacciochini *et al.*, 2010). However, most of these researchers estimated the Stokes number according to the average velocity, and the effects of local velocity were not well considered.

In this study, we use the Stokes number formula proposed by Crowe *et al.* (1985), based on the particle size, the local gas mean velocity, and boundary layer thickness with consideration of the effects of variable plasma properties and non-continuum (Delbos *et al.*, 2006). Our numerical simulation captures the vortex structure caused by the flow around the substrate, and provides for the local boundary layer thickness that the particles pass through before impinging on the substrate. By calculating the particle Saffman lift force, each individual particle can be tracked precisely in its local shear environment. Thus, our simulation results can quantitatively analyze the movement, dispersion, and deposition behaviors of individual particles. Finally, the critical size of particles that follow the plasma jet is deduced, which is consistent with our numerical results under the specific operating conditions.

The spray distance affects the particle parameters significantly in the SPS process. Researchers have studied the effects of spray distances on particle parameters and coating quality (Berghaus *et al.*, 2006; Fazilleau *et al.*, 2006; Fauchais *et al.*, 2008b; Guittienne *et al.*, 2012). But most of these results were chiefly based on experiments, and their conclusions are not mutually consistent. The main reason is that the mechanisms by which the spray distance affects the local flow field and particle movement are not well understood. The effects of spray distance on the flow structures, as well as the particles' heating process, are studied in this paper. The mean velocity and temperature of the particles with their statistical distributions were given for different spray distances, and the proper spray distances are obtained for different micro- and nano-sized particles.

2 Mathematical model

The droplets or particles experienced accelerating and heating in the plasma jet, and a code named LAVA-P-3D was developed to simulate these processes. The plasma gas flow fields were obtained by solving the Navier-Stokes (N-S) equations by the Eulerian method, and tracking the particles as Lagrangian entities.

The N-S equations of the plasma jet were established by assuming that the plasma jets were

continuum, multi-component, compressible, and chemical reacting, with temperature-dependent transport properties in local thermodynamic equilibrium. The turbulence was simulated using the *k-ε* model. Details of the plasma jet simulation may be found in reference (Xiong *et al.*, 2004).

For particles injected into the plasma jet, their aerodynamic force, movement, trajectory, heating, melting, and evaporation were simulated during their flight. Different forces exerted on the particles were considered, including drag force, Saffman lift force, and Brownian force. The corrections for drag coefficient and Nusselt number *Nu* were also considered, taking into account Knudsen effects and the influence of mass evaporation. In a plasma flow field, the volume fraction of particles is less than 10^{-4}, so the effect of collisions between particles was neglected.

2.1 Accelerating and tracking model of particles

For particles in plasma jets, the forces imparted on the particles are mainly the drag force, Saffman lift force, and Brownian force. For particles smaller than 100 μm, the drag force is prominent. For the particles near the jet edge and the substrate, where the flow shear stress is large, the Saffman lift force is significant. For the sub-micron or nano-particles, Brownian force is important. By accounting for these three forces, the acceleration rate of the particles can be expressed as

$$
\begin{aligned}
\boldsymbol{F} &= \boldsymbol{F}_{\text{drag}} + \boldsymbol{F}_{\text{Saffman}} + \boldsymbol{F}_{\text{Brownian}} = m_{\text{p}} \frac{\mathrm{d}V_{\text{p}}}{\mathrm{d}t}, \\
\boldsymbol{F}_{\text{drag}} &= m_{\text{p}} \frac{3}{8} \frac{\bar{\rho}}{\rho_{\text{p}}} \frac{C_{\text{D}}}{r_{\text{p}}} \left| \boldsymbol{V}_{\text{g}} - \boldsymbol{V}_{\text{p}} \right| (\boldsymbol{V}_{\text{g}} - \boldsymbol{V}_{\text{p}}), \\
\boldsymbol{F}_{\text{Saffman}} &= m_{\text{p}} \frac{2K_{\text{c}}(\mu/\rho_{\text{g}})^{0.5} d_{ij}\rho_{\text{g}}}{\rho_{\text{p}} d_{\text{p}} (d_{lk}d_{kl})^{0.25}} (\boldsymbol{V}_{\text{g}} - \boldsymbol{V}_{\text{p}}), \\
\boldsymbol{F}_{\text{Brownian}} &= m_{\text{p}} \boldsymbol{G}_0 \sqrt{\frac{\pi S_0}{\Delta t}},
\end{aligned}
\tag{1}
$$

where $\boldsymbol{F}$ is the total particle force that includes three parts, $\boldsymbol{V}$ is the velocity, m is the mass, d is the diameter, r is the radius, ρ is the density, $\bar{\rho}$ is the turbulent mean density of gas, $\boldsymbol{V}_{\text{g}}$ is the gas velocity within the turbulent fluctuation calculated from the gas turbulence model, and μ is the viscosity. Subscript p means particles or agglomerates, and subscript g means

plasma gas. $K_{\text{c}}=2.594$ is the constant in the Saffman lift force (Saffman, 1965; Aggarwal and Peng, 1995; Chung, 1998), d_{ij} is the deformation tensor as well as d_{lk} and d_{kl}. $\boldsymbol{G}_0$ is a random 3D vector with each number between −1 and 1 and subjected to a Gaussian distribution. S_0 is the spectral intensity, which can be expressed as $S_0 = (216\mu\sigma_{\text{B}}T_{\text{g}})/(32\pi^2 r_{\text{p}}^5 \rho_{\text{p}}^2 C_{\text{c}})$, $\sigma_{\text{B}}=$ 1.38×10^{-23} J/K is the Boltzman constant, T_{g} is the gas temperature, and C_{c} is the Cunningham correction factor. During the particle tracking procedure, the turbulent dispersion of particles is calculated by integrating the trajectory equations for individual particles, using the instantaneous fluid velocity along the particle path. C_{D} is the drag force coefficient expressed by (Chen and Pfender, 1983b)

$$
C_{\text{D}} = \left(\frac{24}{Re_{\text{p}}} + \frac{6}{1+\sqrt{Re_{\text{p}}}} + 0.4 \right) f_{\text{prop}}^{-0.45} f_{Kn}^{0.45},
\tag{2}
$$

where the Reynolds number of the particle is defined as

$$
Re_{\text{p}} = 2\rho_{\text{g}} r_{\text{p}} \left| \boldsymbol{V}_{\text{g}} - \boldsymbol{V}_{\text{p}} \right| / \mu,
\tag{3}
$$

f_{prop} represents the effects of variable plasma properties in the boundary layer surrounding the particle, and can be expressed as $f_{\text{prop}}=\rho_{\text{c}}\mu_{\text{c}}/(\rho_{\text{w}}\mu_{\text{w}})$ (Lee *et al.*, 1981), where subscript c means the cell where the particle is located, and subscript w means the vicinity of particle surface. f_{Kn} is the factor representing Knudsen effect, which can be expressed by

$$
f_{Kn} = \left[1 + \left(\frac{2-a}{a} \right) \left(\frac{\gamma_{\text{w}}}{1+\gamma_{\text{w}}} \right) \frac{4}{Pr} Kn \right]^{-1},
\tag{4}
$$

where *a* is the thermal accommodation factor, usually with the value of 0.8 (Chen and Pfender, 1983a), γ_{w} is the specific heat ratio of gas, *Pr* is the Prandtl number, and *Kn* is the Knudsen number based on the effective mean free path λ, $Kn=\lambda/d_{\text{p}}$, where $\lambda=2\mu/(\rho_{\text{g}}v_{\text{w}})$, v_{w} is the mean molecular speed that is dependent on the gas temperature near the particle surface T_{w} as well as the average molecular weight *W* of the gas mixture, which can be given as $v_{\text{w}}=[8RT_{\text{w}}/(\pi W)]^{1/2}$, where *R* is the gas constant.

For nano-particles, f_{Kn} ranges from 0.005 to 0.1. For the agglomerates and micro-sized particles, f_{Kn} changes from 0.994 to 0.996 (Xiong and Lin, 2009).

Eq. (1) is used to depict the particle velocity and trajectory. The local gas conditions around the particle are employed to calculate its heating.

2.2 Solvent evaporation of droplets

As shown in Fig. 1, the micro- or nano-sized solid particles were assumed to be suspended in the micro-sized droplets randomly. Thermal conduction was neglected in the heating model of the suspension droplets and a lumped thermal capacity model was used, because the Biot number was less than 3×10^{-3} in the present calculation.
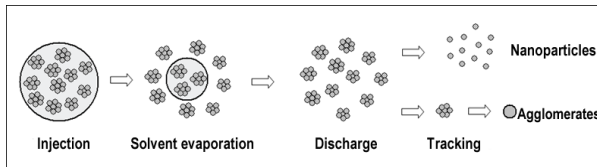
Fig. 1 Schematic of nano-particle injection, discharge, and tracking (Delbos et al., 2006)

The droplet temperature T_d can be expressed by

$$T_d = T_{d,0} + \frac{Q_d}{m_d c_{p,d}} t, \quad \text{if} \quad T_d < T_{m,d},$$

$$T_d = T_{m,d}, \quad \text{if} \quad m_d C_{p,d}(T_{m,d} - T_{d,0}) \le Q_d$$
$$\le m_d C_{p,d}(T_{m,d} - T_{d,0}) + m_d \alpha_{sl} L_{v,sl}, \quad (5)$$

where $T_{d,0}$ is the initial droplet temperature, Q and C_p are the heat gain and specific heat, respectively, T_m is the melting point, α is the weight fraction, and L_v is the latent heat of vaporization. Subscript d means suspension droplet, and subscript sl means solvent. Q_d can be calculated by $Q_d = Q_{conv} - Q_{rad}$, where Q_{conv} represents the convection heat, and Q_{rad} is the radiation heat loss of the particles. $C_{p,d}$ is calculated based on the average of the mass fraction of the solid particle and solvent as $C_{p,d} = C_{p,p}(1 - \alpha_{sl}) + C_{p,sl}\alpha_{sl}$.

When the droplet solvent is totally vaporized, the solid particles contained in the droplet will be discharged into the plasma jet. They might be released as micro-sized agglomerates containing many nano-sized particles or individual nano-sized parti-

cles depending upon the evaporation of the solvent and the aerodynamic forces of the plasma gas (Fauchais and Montavon, 2010). These individual micro- or nano-sized particles are treated as new Lagrangian entities with the current parameters of their mother particle, including position, droplet velocity, and temperature.

2.3 Heating and melting of particles

A 1D model was adopted for the heating and melting of the particle, in which the spherical shape of the particle was assumed as shown in Fig. 2.

Internal convection within the molten part of the particle was not considered. The temperature (T_p) distribution inside the particle was described as

$$\rho_p C_p \frac{\partial T_p}{\partial r} = \frac{1}{r^2} \frac{\partial}{\partial r}\left(k_p r^2 \frac{\partial T_p}{\partial r} \right), \quad (6)$$

where k is the thermal conductivity.

Zero temperature gradient was assumed in the particle center. The particle surface was subjected to the energy conservation law, expressed as (Wan et al., 1999):

$$\left. \frac{\partial T_p}{\partial r} \right|_{r=0} = 0, \quad \text{and}$$

$$4\pi r_p^2 \left(k_p \frac{\partial T_p}{\partial r} \right)\Bigg|_{r=r_p} = \dot{Q}_{conv} - \dot{Q}_{vap} - \dot{Q}_{rad}, \quad (7)$$

where the convection, evaporation latent, and radiation heat rates ($\dot{Q}_{conv}$, $\dot{Q}_{vap}$, and $\dot{Q}_{rad}$) are expressed as $4\pi r_p^2 h_f(T_f - T_s)$, $\dot{m}_v L_v$, and $4\pi r_p^2 \varepsilon_p \sigma_s(T_s^4 - T_\infty^4)$, respectively. T_s is the particle surface temperature, $\dot{m}_v$ is the vaporization rate, ε_p is the particle surface emissivity coefficient, σ_s is the Stefan-Boltzmann constant, and T_∞ is the temperature outside boundary layer. The film temperature T_f was defined as $(T_s + T_g)/2$, as shown in Fig. 2, which is introduced to deal with the steep temperature gradient in the boundary layer around the particle. Only the radiation between the particle surface and the environment was considered in the case of optically thin plasma gas. The heat transfer coefficient, h_f, can be calculated from (Chen and Pfender, 1982)

$$Nu = \frac{2h_f r_p}{k_f} = \left(2.0 + 0.6 Re_p^{1/2} Pr^{1/3}\right) f_{\mathrm{prop}} f_{Kn} f_v, \quad (8)$$

where k_f is thermal conductivity of the film around the particle, f_v accounts for the effect of mass transfer due to evaporation, which can be found in reference (Xiong and Lin, 2009). Additional constraints of energy balance between the heat conduction and latent heat at the melting interface r_m were also considered:

$$\left(k_p \frac{\partial T_p}{\partial r}\right)\Bigg|_{r=r_m^-} - \left(k_p \frac{\partial T_p}{\partial r}\right)\Bigg|_{r=r_m^+} = L_m \rho_p \frac{dr_m}{dt}. \quad (9)$$
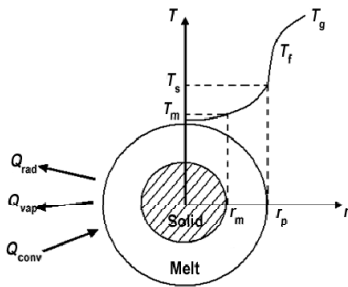
Fig. 2 Schematic of particle heat transfer

3 Experimental and numerical setup

This study was conducted for a direct-current (DC) suspension plasma spray system with axial injection of feedstock as shown in Fig. 3. The injection point was at $x=0$, $y=0.1$, and $z=0$, and the injection direction was given by a random distribution from 0° to 20° with regard to y-axis. Gas mixtures of argon and hydrogen were ionized in a plasma gun to form a high temperature and high velocity plasma jet. The droplets and particles were accelerated and heated in the plasma field. Finally, the melting particles formed coatings on the substrate. Operating parameters of this gun are listed in Table 1.

Different diameters of ZrO_2 particles from 10 nm to 1 μm were suspended in the ethanol solvent as shown in Fig. 1. The particle properties are listed in Table 2 and the solvent properties in Table 3.

At the nozzle exit, the velocity and temperature can be expressed by the empirical formulae

(Ramshaw and Chang, 1992) $v(r) = V_{cl}[1-(r/R_i)^{1.2}]$ and $T(r) = (T_{cl} - T_w)[1-(r/R_i)^6] + T_w$, where V_{cl} and T_{cl}
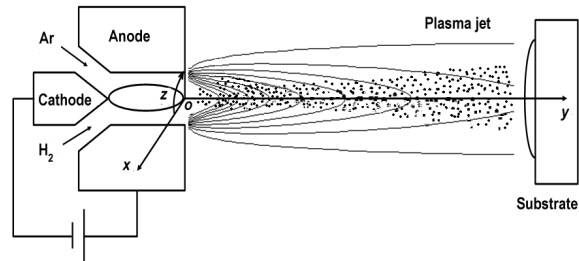

Fig. 3 Schematic of the DC plasma spray

Table 1 Baseline operating conditions of single particle injection

Processing parameter	Value
Plasma gas conditions	
Total plasma gas flow rate (SLM)*	80
Gas composition (Ar, H₂) (%)	85, 15
Power input (kW)	30
Feedstock conditions (ZrO₂)	
Solid content in suspension (%)	10
Initial nano-particle size (nm)	10, 800, 1000
Initial suspension droplet radius (μm)	25
Spray distance (cm)	5, 8

* SLM means standard liter per minute; 1 SLM=16.67 cm³/s

Table 2 Particle properties (ZrO₂) (Xiong and Lin, 2009)

| Parameter	Value
Solid density (kg/m³)	5.89×10^3
Solid thermal conductivity (W/(m·K))	2.0
Liquid thermal conductivity (W/(m·K))	3.0
Solid specific heat (J/(kg·K))	580
Liquid specific heat (J/(kg·K))	713
Melting temperature (K)	2950
Boiling temperature (K)	5000
Latent heat of melting (J/kg)	8×10^5
Latent heat of vaporization (J/kg)	6×10^6

Table 3 Solvent properties (ethanol) (Xiong and Lin, 2009)

Parameter	Value
Density (kg/m³)	0.8×10^3
Specific heat (J/(kg·K))	2400
Latent heat of vaporization (J/kg)	9.25×10^5
Boiling temperature (K)	351

are the velocity and temperature along the nozzle exit with the orifice radius R_i=0.4 cm, respectively, and are calculated from the total amount of momentum and thermal energy transferred to the plasma jet. T_w is the wall temperature with an initial value of 300 K, and the velocity at the wall boundary is 0. The downstream of the jet flow is open.

The plasma flow field was solved using a cylindrical coordinate system. The radial distance was 6 cm with 57 grid points, and the axial distance was 15 cm with 66 grid points. The droplets and particles were tracked in the plasma flow field. The particle temperature distribution and location of the melting interface were calculated using 50 grid points in spherical coordinates. The droplets had an initial temperature of 300 K and a velocity of 50 m/s. A typical mean droplet size of 50 μm was assigned based on the commonly used pneumatic atomizer (Xiong and Lin, 2009).

4 Validation of model predictions

To verify the numerical code LAVA-P-3D for the plasma spray process, the centerline gas temperature profiles were calculated and compared with published numerical results (Jabbari *et al.*, 2014) and experimental data (Brossa and Pfender, 1988) in Fig. 4. A good agreement between the simulation results and experimental data was obtained. The deviation between experiment and our modeling result is within 10%. Both experiment and simulation used the Sulzer 3MB plasma gun with the same operating parameters as in reference (Jabbari *et al.*, 2014).
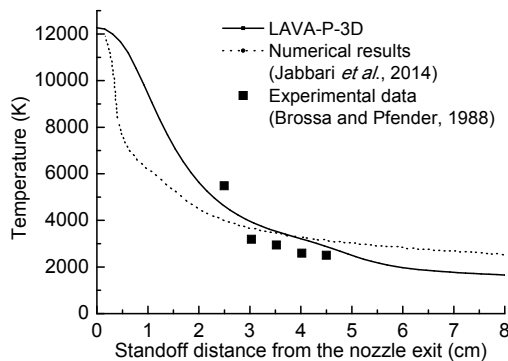
Fig. 4 Comparison of centerline gas temperature profiles with published numerical results (Jabbari *et al.*, 2014) and experimental data (Brossa and Pfender, 1988)

5 Discussion

5.1 Plasma jet

Fig. 5 shows the plasma field velocity and temperature contours as well as the streamlines. The hot core was downstream of the nozzle exit within an axial spray distance of about 1 cm, where the gas temperature was as high as 10 000 K and the velocity was up to 3000 m/s. Beyond this region, the gas velocity decelerated and the temperature cooled down continuously along the spray distance. The dark plate located at the distance of 5 cm in Fig. 5 represents the substrate wall. The gas flowed around the substrate and formed two vortexes behind the substrate and another two vortexes on the wall shoulders. The vortexes on the shoulders were formed because of a steep shear layer at the outer edge of the jet, and the flow separation induced those two vortexes behind the substrate. The vortexes behind the substrate had low gas velocity, where small particles might get entrained on the back of the substrate.
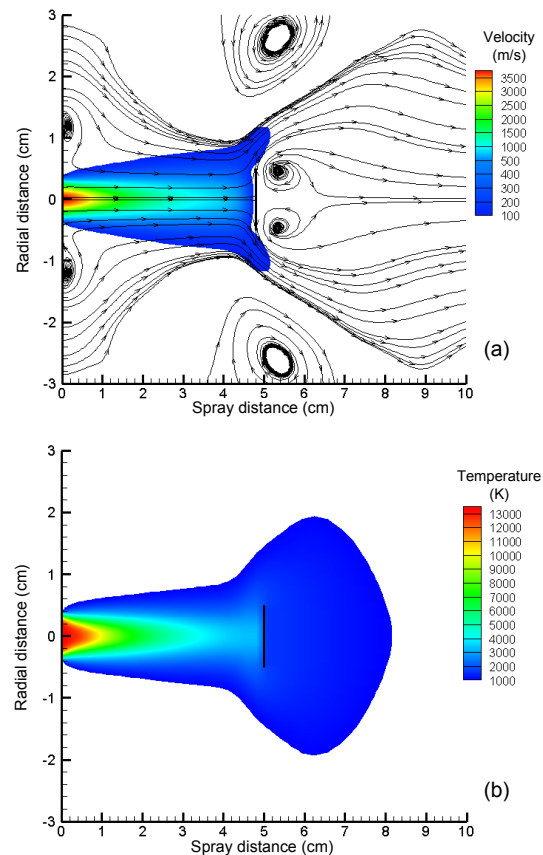
Fig. 5 Gas velocity contours with streamlines (a) and temperature contours in the mid-plane of the plasma jet (b)

5.2 Motion of the particles

Particle motion is complex in an SPS. Fig. 6 depicts the snapshots of particles in the mid-plane at different times from 0.01 ms to 0.06 ms. It shows how the particles move along the spray distance after injection. From 0.01 ms to 0.03 ms, the particles near the axis have higher axial velocity and smaller radial velocity than those in the periphery. Therefore, the particle traces form a cone shape that accords well with the streamlines of a jet flow field as shown in Fig. 5. At 0.04 ms, the spatial distribution of the particles becomes flatter. This is because in the downstream of the plasma field, the axial particle velocity becomes zero due to deceleration by the substrate. From 0.05 ms to 0.06 ms, the particles begin to move along the substrate, and the radial distribution becomes wider and wider, especially for the peripheral particles. This is because the radial particle velocity near the substrate becomes larger and larger as the gas flow separates at the substrate edge.
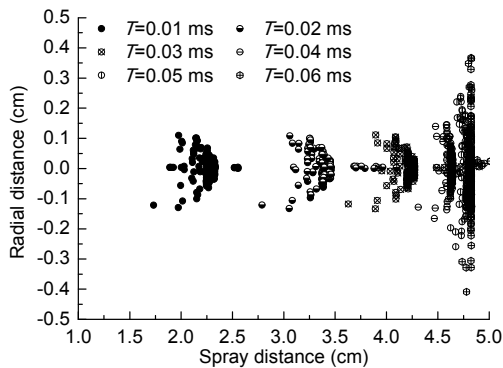

**Fig. 6 Snapshots of 100 nm particles in the mid-plane of the spray at different times**

Fig. 7 represents the radial velocity of single particles with different diameters of 10 nm, 100 nm, and 1 μm. From the picture, we can see the radial velocity of the 10 nm particle fluctuates sharply due to the effect of Brownian force, while that of the micro-sized particle shows less fluctuation.

For nano-sized particles, the Brownian force affects their velocities and trajectories significantly at each instantaneous moment. In this study, we considered the effect of Brownian force on the motion history of an individual particle (Shao *et al.*, 2015).

The distributions of multiple particles on the substrate with and without Brownian force were also studied, and the results for the 10 nm particles are shown in Fig. 8.
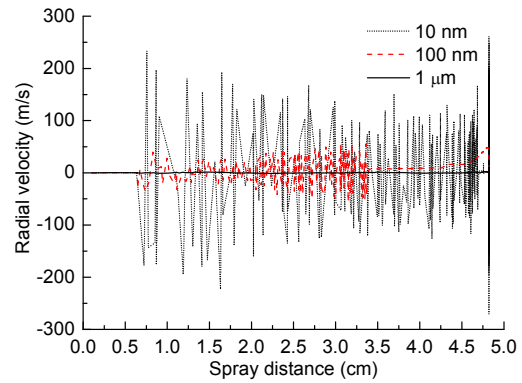
Fig. 7 Radial velocity of particles with different diameters of 10 nm, 100 nm, and 1 μm
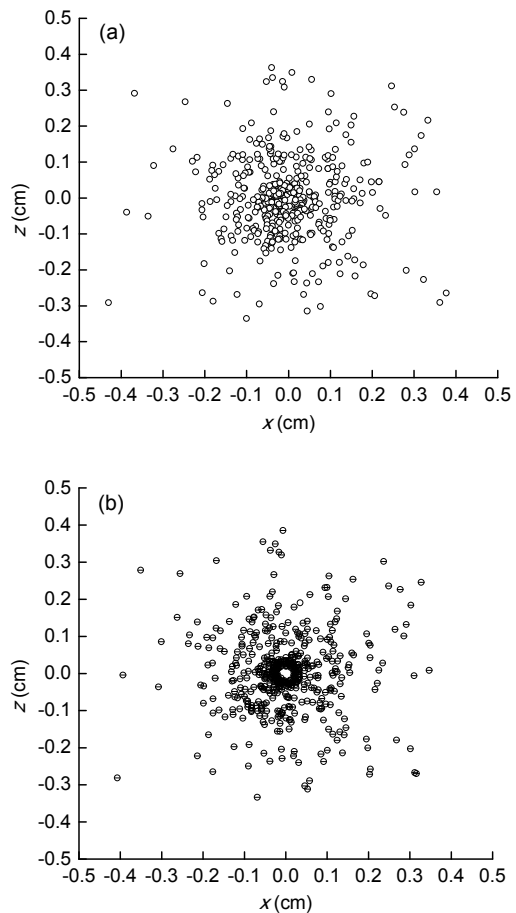
Fig. 8 Distribution of nano-sized particles in the vertical plane with (a) and without (b) Brownian force

The spatial ranges were wider when considering the Brownian force compared with the case without Brownian force. Moreover, more particles were distributed in the periphery of the spray, and particles were scattered more evenly in the center of the spray. This is because the Brownian force leads the nano-particles to distribute more homogeneously.

5.3 Stokes number and critical particle diameter

Particles with different diameters move along different trajectories when impinging on the substrate. The Stokes number (St) is an important parameter in characterizing the trajectory of particle.

Using the formula by Crowe *et al.* (1985; 1988) as $St = \rho_p d_p^2 U / (18 \mu L)$ with gas viscosity of about 5×10^{-5} kg/(m·s) for the mixture of argon and hydrogen near the substrate boundary layer, with gas velocity near the boundary layer of U=24 m/s, boundary layer thickness of L=0.1 mm, and consideration of the Reynolds number near the substrate, we calculated that the critical particle diameter was 780 nm (about 800 nm), corresponding to St=1. This means that particles smaller than 800 nm will not have enough inertia to penetrate the viscous boundary layer and will fly away with the flow. Particles larger than 800 nm are more likely to be captured by the substrate. The above Stokes number formula including the information on local gas velocity and local boundary layer can be used to estimate the critical diameter for a particle that follows the flow.

To demonstrate the critical particle diameter of 800 nm, we tracked numerically three particles around the substrate, with diameters of 10 nm, 800 nm, and 10 μm, as shown in Fig. 9. The 10 nm particle moved along the axis of the flow field at first. As it moved toward the substrate, it was entrained and kept spinning inside the vortexes behind the substrate. The scale of the spinning circle was comparable to the vortex size of the gas flow, and the trajectory reflected the flow structures near the substrate. The 800 nm particle followed the gas flow and moved over the substrate, but it would not enter the vortex as the 10 nm particle because of its larger inertia. The 10 μm particle could not flow over the substrate and, instead, moved near the axis and impacted directly on the substrate. Therefore, our numerical results of particle movement around the substrate agree well with the analysis using the Stokes number.

5.4 Effects of the substrate wall

The spray distance from the nozzle exit to the substrate is a key parameter that affects the flow structure, as well as the acceleration and heating of the particles, and the substrate also affects their distribution. Nano-particles are easily centrifuged away from the center region by the plasma flow near the substrate. Because of the existence of the substrate, there was a hollow area at the center. This phenomenon also indicated that the substrate affects the distribution of particles downstream.
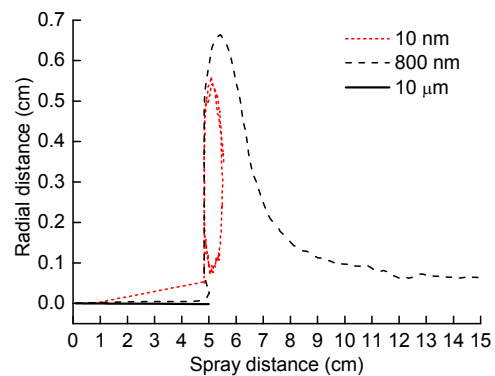

Fig. 9 Trajectories of particles with different diameters of 10 nm, 800 nm, and 10 μm

Particle distributions at different spray distances are shown in Fig. 10. These particles had the same diameter of 10 nm, and the locations of the substrate were 5 and 8 cm from the nozzle exit. More particles were collected at the center of the substrate located at 5 cm. There were 10% more particles at the center in the small distance case, and the spread domain was smaller than that with a substrate at 8 cm. The reason for this difference is that when the substrate is located near the nozzle, the gas velocity is larger, and more particles can penetrate the stagnation flow near the substrate and adhere to it. In addition, for the substrate located at 5 cm, the average temperature of the particles when they impacted on the substrate was 3215 K, which was higher than the melting temperature of ZrO_2, whereas, when the spray distance was 8 cm, the highest particle temperature was 2465 K, and particles were thus not molten when they impacted on the substrate. So the deposition rate was higher when the substrate was located at a spray distance of 5 cm, than when it was located at 8 cm. If the spray distance is too short, particles may not be sufficiently heated, while if the distance is too
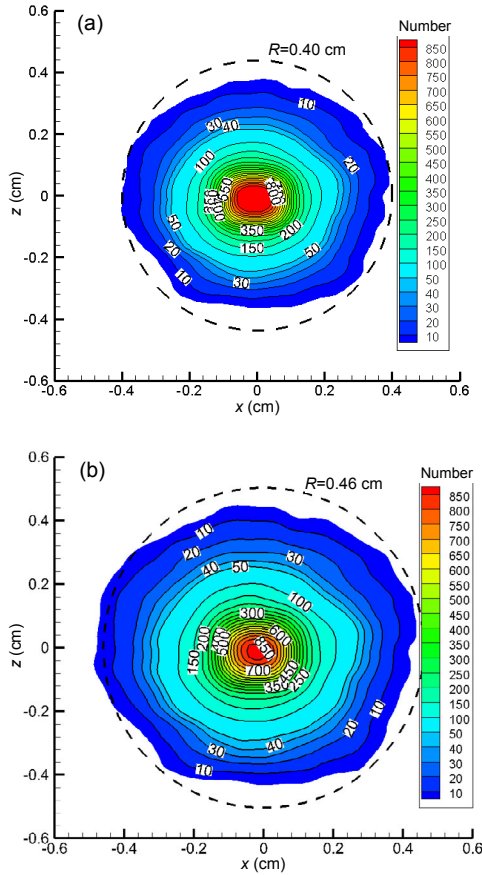
Fig. 10 Distribution of nano-sized particles in the vertical plane at spray distances of 5 cm (a) and 8 cm (b)

long, the particles will lose some of their momentum and energy before impact, due to the cooling of the jet. Plasma spray processes under the above two conditions produce poor quality coatings.
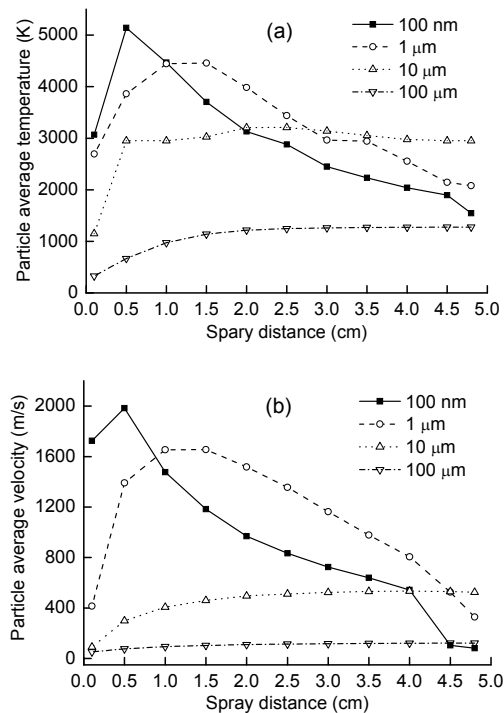
5.5 Effects of particle size

The sizes of particles will affect their temperature and velocity. Fig. 11 shows the average temperature and velocity for four different particle diameters ranging from 100 nm to 100 μm. From Fig. 11, we can see that these four diameters of particles experienced different motion processes. The 100 nm particles got heated and accelerated more rapidly than the micron particles. However, in the downstream of flow field, the micron particles had greater velocity and higher temperature. This is because the micro-sized particles had larger inertia and heat capacity than the nano-particles. The 10 and 100 μm particles were always accelerating and getting heated. Besides, the larger the particle was, the longer the

process lasted. Under the chosen conditions, the 10 μm particles could reach their melting temperature.

The radial distributions of multiple nano-particles and micro-sized particles are shown in Fig. 12. Their diameter ranges were from 100 nm to 1 μm, and from 1 μm to 100 μm for nano-particles and micro-sized particles, respectively. The radial distribution range of micron particles was smaller than that of the nano-particles by 0.1 cm. This is because the Brownian force plays a more significant role for nano-particles than for micron particles. The percentage of micro-sized particles gathered near the center (radial distance smaller than 0.1 cm) was 87%, compared with 71% for nano-particles.

The temperatures and velocities of different sized particles are shown in Figs. 13 and 14, respectively. The average temperature and velocity of micro-sized particles are larger than those of nano-particles. The reason is that the micron particles have larger inertia and heat capacity than the nano-particles. The standard deviations (σ) of the radial distribution of temperature and velocity of the micron particles were larger, because the micron particles covered diameters from 1 μm to 100 μm, while the nano or sub-micrometer contained only two different size orders.

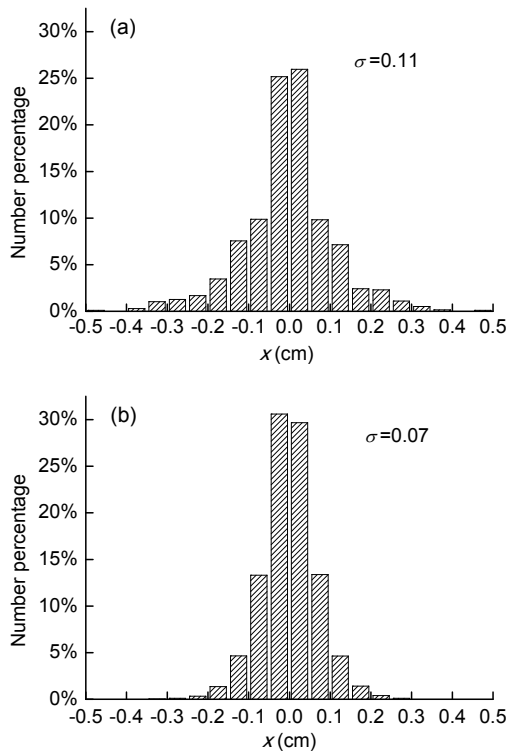**Fig. 11 Effects of particle sizes on their average temperature (a) and velocity (b)**

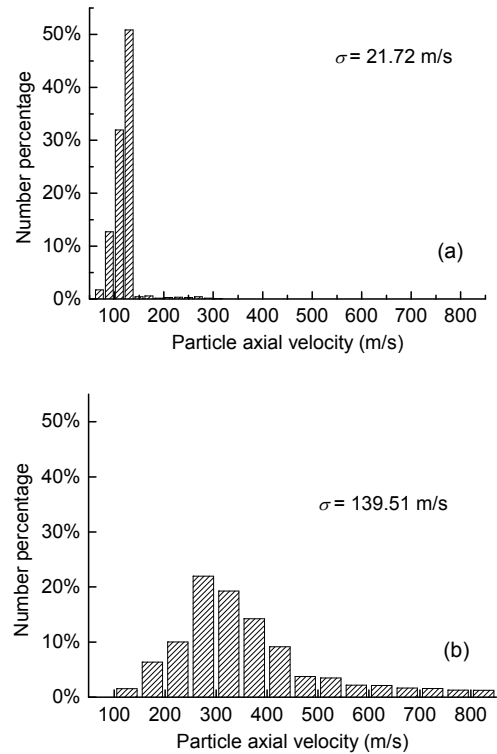**Fig. 12 Radial distribution of nano-particles (a) and micro-sized particles (b)**

Fig. 13 Distribution of temperatures for nano-particles (a) and micro-sized particles (b)

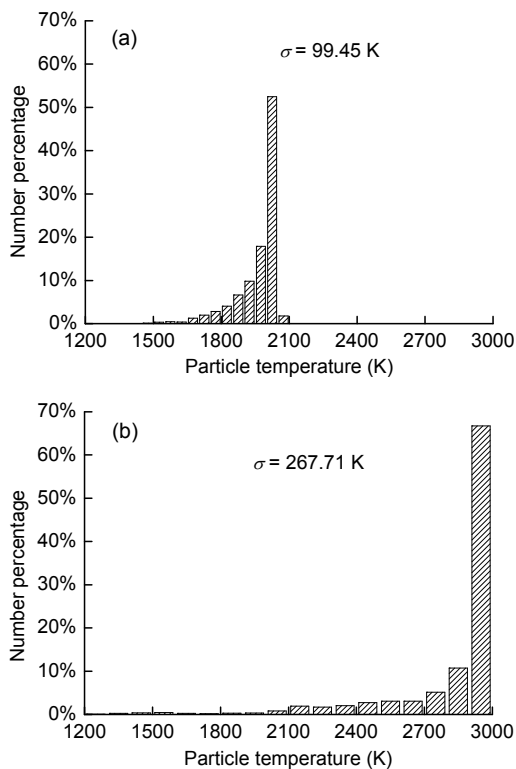**Fig. 14 Distribution of axial velocities for nano-particles (a) and micro-sized particles (b)**

6 Conclusions

In this study, a comprehensive model has been developed to simulate the trajectories and acceleration of different sized particles, and their heating, melting, and evaporation processes. This model is suitable for simulating the behaviors of both nano-particles and sub-micro-sized particles. Both Stokes number and the spray distance as key parameters affecting the particle motion were investigated. Besides, the dynamic processes of multiple particles were studied. The following conclusions can be drawn:

1. For the nano-sized particles, the Brownian force affects their distribution, and the present model can simulate the behaviors of those small particles.

2. There is a critical particle diameter corresponding to Stokes number equal to 1, to identify the trajectory of the particle around the substrate. In this study, the critical particle diameter that will follow the flow field is about 800 nm.

3. In the downstream of the plasma jet, the substrate affects the flow structures and spatial distribution

of the particles. In this study, we identify the spray distance that achieves the ideal deposition quality, which is about 50 mm for nano-particles, and should be larger for micron particles.

4. The spatial distributions of nano-particles and micron particles are different. The nano-particles have wider distribution ranges than those of the micron particles. The Brownian motion is more significant for nano-particles than that for micron particles.

5. The acceleration and heating processes are different for nano-particles and micron particles. The nano-particles have smaller inertia and heat capacity than micron particles, so their velocity and temperature change more rapidly.

References

Aggarwal, S.K., Peng, F., 1995. A review of droplet dynamics and vaporization modeling for engineering calculations. *Journal of Engineering for Gas Turbines and Power*, **117**(3):453-461.
http://dx.doi.org/10.1115/1.2814117

Bacciochini, A., Ilavsky, J., Montavon, G., *et al.*, 2010. Quantification of void network architectures of suspension plasma-sprayed (SPS) yttria-stabilized zirconia (YSZ) coatings using ultra-small-angle X-ray scattering (USAXS). *Materials Science and Engineering: A*, **528**(1):91-102.
http://dx.doi.org/10.1016/j.msea.2010.06.082

Berghaus, J.O., Marple, B., Moreau, C., 2006. Suspension plasma spraying of nanostructured WC-12Co coatings. *Journal of Thermal Spray Technology*, **15**(4):676-681.
http://dx.doi.org/10.1361/105996306X147072

Brossa, M., Pfender, E., 1988. Probe measurements in thermal plasma jets. *Plasma Chemistry and Plasma Processing*, **8**(1):75-90.
http://dx.doi.org/10.1007/BF01016932

Chen, X., Pfender, E., 1982. Heat transfer to a single particle exposed to a thermal plasma. *Plasma Chemistry and Plasma Processing*, **2**(2):185-212.
http://dx.doi.org/10.1007/BF00633133

Chen, X., Pfender, E., 1983a. Effect of the Knudsen number on heat transfer to a particle immersed into a thermal plasma. *Plasma Chemistry and Plasma Processing*, **3**(1): 97-113.
http://dx.doi.org/10.1007/BF00566030

Chen, X., Pfender, E., 1983b. Behavior of small particles in a thermal plasma flow. *Plasma Chemistry and Plasma Processing*, **3**(3):351-366.
http://dx.doi.org/10.1007/BF00564633

Chung, K.C., 1998. Three-dimensional analysis of airflow and contaminant particle transport in a partitioned enclosure. *Building and Environment*, **34**(1):7-17.
http://dx.doi.org/10.1016/S0360-1323(97)00073-5

Crowe, C.T., Gore, R.A., Troutt, T.R., 1985. Particle dispersion by coherent structures in free shear flows. *Particulate Science and Technology*, **3**(3-4):149-158.
http://dx.doi.org/10.1080/02726358508906434

Crowe, C.T., Chung, J.N., Troutt, T.R., 1988. Particle mixing in free shear flows. *Progress in Energy and Combustion Science*, **14**(3):171-194.
http://dx.doi.org/10.1016/0360-1285(88)90008-1

Delbos, C., Fazilleau, J., Rat, V., *et al.*, 2006. Phenomena involved in suspension plasma spraying part 2: zirconia particle treatment and coating formation. *Plasma Chemistry and Plasma Processing*, **26**(4):393-414.
http://dx.doi.org/10.1007/s11090-006-9020-8

Faeth, G.M., 1987. Mixing, transport and combustion in sprays. *Progress in Energy and Combustion Science*, **13**(4):293-345.
http://dx.doi.org/10.1016/0360-1285(87)90002-5

Fauchais, P., 2004. Understanding plasma spraying. *Journal of Physics D: Applied Physics*, **37**(9):R86-R108.
http://dx.doi.org/10.1088/0022-3727/37/9/R02

Fauchais, P., Montavon, G., 2010. Latest developments in suspension and liquid precursor thermal spraying. *Journal of Thermal Spray Technology*, **19**(1-2):226-239.
http://dx.doi.org/10.1007/s11666-009-9446-7

Fauchais, P., Rat, V., Coudert, J.F., *et al.*, 2008a. Operating parameters for suspension and solution plasma-spray coatings. *Surface and Coatings Technology*, **202**(18): 4309-4317.
http://dx.doi.org/10.1016/j.surfcoat.2008.04.003

Fauchais, P., Etchart-Salas, R., Rat, V., *et al.*, 2008b. Parameters controlling liquid plasma spraying: solutions, sols, or suspensions. *Journal of Thermal Spray Technology*, **17**(1):31-59.
http://dx.doi.org/10.1007/s11666-007-9152-2

Fazilleau, J., Delbos, C., Rat, V., *et al.*, 2006. Phenomena involved in suspension plasma spraying part 1: suspension injection and behavior. *Plasma Chemistry and Plasma Processing*, **26**(4):371-391.
http://dx.doi.org/10.1007/s11090-006-9019-1

Guittienne, P., Grange, D., Hollenstein, C., *et al.*, 2012. Plasma jet-substrate interaction in low pressure plasma spray-CVD processes. *Journal of Thermal Spray Technology*, **21**(2):202-210.
http://dx.doi.org/10.1007/s11666-011-9702-5

Huang, P.C., Heberlein, J., Pfender, E., 1995. Particle behavior in a two-fluid turbulent plasma jet. *Surface and Coatings Technology*, **73**(3):142-151.
http://dx.doi.org/10.1016/0257-8972(94)02382-4

Jabbari, F., Jadidi, M., Wuthrich, R., *et al.*, 2014. A numerical study of suspension injection in plasma-spraying process. *Journal of Thermal Spray Technology*, **23**(1-2):3-13.
http://dx.doi.org/10.1007/s11666-013-0030-9

Jen, T.C., Li, L., Cui, W., *et al.*, 2005. Numerical investigations on cold gas dynamic spray process with nano- and microsize particles. *International Journal of Heat and Mass Transfer*, **48**(21-22):4384-4396.
http://dx.doi.org/10.1016/j.ijheatmasstransfer.2005.05.008

Jordan, E.H., Xie, L., Gell, M., *et al.*, 2004. Superior thermal barrier coatings using solution precursor plasma spray. *Journal of Thermal Spray Technology*, **13**(1):57-65. http://dx.doi.org/10.1007/s11666-004-0050-6

Lee, Y.C., Hsu, K.C., Pfender, E., 1981. Modeling of particles injected into a DC plasma jet. Proceedings of the 5th International Symposium on Plasma Chemistry, Edinburgh, UK, p.795.

Meillot, E., Damiani, D., Vincent, S., *et al.*, 2013a. Analysis by modeling of plasma flow interactions with liquid injection. *Surface and Coatings Technology*, **220**:149-156. http://dx.doi.org/10.1016/j.surfcoat.2012.11.025

Meillot, E., Vincent, S., Caruyer, C., *et al.*, 2013b. Modelling the interactions between a thermal plasma flow and a continuous liquid jet in a suspension spraying process. *Journal of Physics D*: Applied Physics, **46**(22):224017. http://dx.doi.org/10.1088/0022-3727/46/22/224017

Pateyron, B., Pawłowski, L., Calve, N., *et al.*, 2013. Modeling of phenomena occurring in plasma jet during suspension spraying of hydroxyapatite coatings. *Surface and Coatings Technology*, **214**:86-90. http://dx.doi.org/10.1016/j.surfcoat.2012.11.006

Pfender, E., 1989. Particle behavior in thermal plasmas. *Plasma Chemistry and Plasma Processing*, **9**(S1):167S-194S. http://dx.doi.org/10.1007/BF01015878

Ramshaw, J.D., Chang, C.H., 1992. Computational fluid dynamics modeling of multicomponent thermal plasmas. *Plasma Chemistry and Plasma Processing*, **12**(3):299-325. http://dx.doi.org/10.1007/BF01447028

Saffman, P.G., 1965. The lift on a small sphere in a slow shear flow. *Journal of Fluid Mechanics*, **22**(02):385-400. http://dx.doi.org/10.1017/S0022112065000824

Shao, X., Zhang, K., Xiong, H., 2015. Modeling of micro- and nanoparticle characteristics in DC suspension plasma spray. *Journal of Thermal Spray Technology*, **24**(3): 309-317. http://dx.doi.org/10.1007/s11666-014-0182-2

Wan, Y.P., Prasad, V., Wang, G.X., *et al.*, 1999. Model and powder particle heating, melting, resolidification, and evaporation in plasma spraying processes. *Journal of Heat Transfer*, **121**(3):691-699. http://dx.doi.org/10.1115/1.2826034

Xiong, H.B., Lin, J.Z., 2009. Nanoparticles modeling in axially injection suspension plasma spray of zirconia and alumina ceramics. *Journal of Thermal Spray Technology*, **18**(5-6):887-895. http://dx.doi.org/10.1007/s11666-009-9349-7

Xiong, H.B., Zheng, L.L., Sampath, S., *et al.*, 2004. Three-dimensional simulation of plasma spray: effects of carrier gas flow and particle injection on plasma jet and entrained particle behavior. *International Journal of Heat and Mass Transfer*, **47**(24):5189-5200. http://dx.doi.org/10.1016/j.ijheatmasstransfer.2004.07.005

Xiong, H.B., Zheng, L.L., Li, L., *et al.*, 2005. Melting and oxidation behavior of in-flight particles in plasma spray process. *International Journal of Heat and Mass Transfer*, **48**(25-26):5121-5133. http://dx.doi.org/10.1016/j.ijheatmasstransfer.2005.07.019

Ye, R., Proulx, P., Boulos, M.I., 2000. Particle turbulent dispersion and loading effects in an inductively coupled radio frequency plasma. *Journal of Physics D: Applied Physics*, **33**(17):2154-2162. http://dx.doi.org/10.1088/0022-3727/33/17/310

中文概要

题　　目： 悬浮等离子体喷涂过程中微纳米颗粒撞击基板的动力学模拟

目　　的： 研究微纳米颗粒在流场中的运动和传热特性，确定颗粒绕流的临界尺寸以及微纳米颗粒合适的喷涂距离。

创新点： 1. 建立微纳米颗粒的受力和运动模型；2. 推导颗粒粒径和斯托克斯数的关系，确定颗粒绕流的临界尺寸；3. 确定适于微纳米颗粒的喷涂距离。

方　　法： 1. 通过颗粒运动和传热的三维模型，模拟颗粒在等离子体流场中的运动和传热过程；2. 对流场采用欧拉法进行求解，对颗粒采用拉格朗日法进行求解；3. 动态追踪颗粒的轨迹和空间分布，从而得到颗粒的速度、温度和空间分布。

结　　论： 1. 布朗力会影响纳米颗粒的分布；现有模型可以很好地模拟微纳米颗粒的行为。2. 可以用斯托克斯数和粒径表征微纳米颗粒绕流的临界尺寸；当前工况下，临界粒径约为 800 nm。3. 基板会影响流场结构和颗粒的空间分布；在当前研究中，得出有利于纳米颗粒沉积的喷涂距离约为 50 mm；对微米颗粒来说，喷涂距离应适当增大。4. 微纳米颗粒的空间分布呈现不同的特点；纳米颗粒的分布区间更大，布朗力对纳米颗粒的作用比对微米颗粒更为显著。5. 微纳米颗粒的运动和传热过程呈现不同的特点；纳米颗粒的惯性和热容小，因此它们的速度和温度变化更迅速。

关键词： 悬浮等离子体喷涂；斯托克斯数；布朗力；多相流；固体-流体相互作用